ISSN: 2414-1895 DOI: 10.6919/ICJE.202504_11(4).0042

Study on the Consequent-Pole Linear Motor with Magnetically Conductive Blocks in the Primary Stage

Xuanfeng Shangguan, Qi Wang, Xin Wang, Yu Xie

School of Electrical Engineering and Automation, Henan Polytechnic University, Jiaozuo 454000, China

Abstract

A new structure U-type permanent magnet linear synchronous motor is proposed and analyzed. The secondary permanent magnet pole potential function and the air-gap specific permeability function are established to find the analytical solution of the no-load magnetic field of the motor by the method of the road, and the harmonic analysis of the air-gap flux density (radial component) is carried out. The finite element method is used to analyze the influence of some structural parameters of the motor on electromagnetic thrust and thrust fluctuation, and the sensitivity analysis of structural parameters is done by Taguchi's experimental design method to determine the optimization variables. The response surface method is used to obtain the fitting function between thrust, thrust fluctuation and optimization variables. With thrust and thrust fluctuation as the optimization objectives, the multi-objective optimization design of the motor is carried out using the White Heron algorithm. The finite element analysis results verify the validity of the theoretical analysis.

Keywords

U-type Permanent Magnet Synchronous Linear Motor; Magnetic Potential Function; Specific Magnetic Permeability; Multi-objective Optimization Design.

1. Introduction

Permanent magnet synchronous linear motors have become an important development direction for linear motors due to their simple structure, flexible installation, good dynamic performance, high efficiency and power factor[1-3]. Ironless core permanent magnet synchronous linear motors have the advantages of fast response speed, low thrust fluctuation and high positioning accuracy, and are widely used in high-precision fields such as CNC machine tools and semiconductor manufacturing [4-7]. However, the primary of this motor does not have an iron core and has a low thrust density, resulting in limited applications. Therefore, increasing thrust has become a research priority in the field of coreless linear motors. Literature [8] optimized the motor parameters to improve the thrust of the motor by performing electromagnetic-thermal coupling analysis of the motor. Literature [9] prevented the air gap flux density from decreasing by studying the magnetic field distribution in the back iron of the motor and reducing the magnetic saturation of the back iron. Literature [10] proposes a Halbach-structured coreless permanent magnet synchronous linear motor, where the use of Halbach arrays for the permanent magnets can increase the air-gap flux density and improve its distribution, thus increasing the thrust of the motor. In addition, the climbing price of permanent magnet materials has increased the manufacturing cost of motors, limiting the application of permanent magnet linear motors[11]. Therefore, it is very important to improve the utilization rate of permanent magnet materials and reduce the production cost.

The alternating pole motor model was proposed in 1985[12], which was favored for its low cost and high utilization of permanent magnets by replacing some of the permanent magnet poles by using

ISSN: 2414-1895 DOI: 10.6919/ICJE.202504_11(4).0042

convex poles composed of ferromagnetic materials [13]. Scholars in the motor community at home and abroad have studied the application of alternating pole structures to permanent magnet linear motors. Literature

[14] compares alternating-pole permanent magnet synchronous linear motors with conventionally constructed motors and shows that alternating-pole motors have higher permanent magnet utilization. Literature [15] proposes a Halbach alternating pole permanent magnet linear motor to further improve the thrust of the motor and reduce the thrust fluctuation. Literature [16] proposes a trapezoidal Halbach alternating-pole permanent magnet synchronous linear motor, which has higher utilization of trapezoidal-structured permanent magnets and lower thrust fluctuations compared to rectangular Halbach permanent magnet arrays.

In this paper, a new structural form is proposed based on the coreless linear motor: (1) the fixed secondary adopts alternating magnetic poles; (2) the moving primary is embedded with a magnetic guide block. Such a structure improves the motor's thrust density and permanent magnet material utilization.

2. Motor Structure

The structure of the motor is shown in Fig. 1, which is mainly composed of two parts: primary and secondary. The motor adopts long secondary and short primary structure. The primary consists of windings and magnetic conductor blocks molded in epoxy resin, and the secondary consists of magnetic poles and back iron. The motor has a bilateral secondary structure and is “U” shaped. Each pair of poles of the motor consists of a permanent magnet pole and a convex iron pole. The convex iron poles are magnetized into anisotropic poles by adjacent permanent magnet poles, and the permanent magnet poles and convex iron poles are arranged alternately. Fig. 1(b) represents the magnetization direction and flux path of the permanent magnet pole. In addition, the magnetizing block added in the primary can act as a magnetizer to increase the thrust of the motor. The motor adopts 8-pole 9-slot centralized winding.

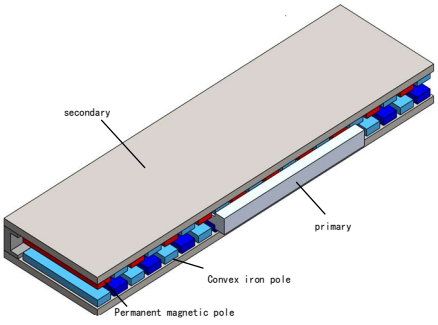

(a)three-dimensional model

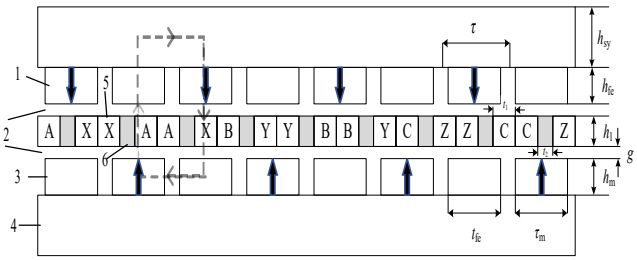

(b)2D structural diagram

1-Permanent magnetic pole 2-Air gap 3-Convex iron pole 4- Secondary iron 5-Primary winding 6-Magnetic guide block

Fig. 1 Consequent-Pole Linear Motor with Magnetically Conductive Blocks in the Primary Stage

ISSN: 2414-1895 DOI: 10.6919/ICJE.202504_11(4).0042

3. Air Gap Magnetic Density Analysis

In this paper, the no-load air-gap magnetic field is solved by the method of magnetic circuit, and the no-load air-gap magnetic field of the motor is computationally analyzed by establishing the magnetic potential function and specific permeability function of the motor [17]. The structural parameters of the original prototype are shown in Table 1.

Table 1. Structural parameters of the original prototype

Parameter	Value	Parameter	Value
Coil side width t_1/mm	5.5	Permanent magnet width τ_m/mm	14
Coil edge height h_1/mm	7.21	Permanent magnet height h_m/mm	6
Width of magnetic guide block t_2/mm	5	Current density J/A·mm^{-2}	6
Height of magnetic guide block h_2/mm	7.21	Height of air gap g/mm	0.84
Polar distance τ/mm	18	Motor width d/mm	50
Primary length l/mm	144	Convex iron pole width t_{fe}/mm	14
Secondary back iron thickness h_{sy}/mm	10	Convex iron pole height h_{fe}/mm	6

In order to simplify the analytical model, the following assumptions are made:

(1) the motor is extended infinitely along the x-axis direction and the longitudinal end effect is neglected;

(2) Neglect the inter-pole leakage flux;

(3) The permeability of ferromagnetic material is taken as infinity;

(4) The relative permeability of the permanent magnet is taken as 1.

3.1 Permanent Magnetic Pole Potential

According to the arrangement order of the permanent magnets can be obtained the magnetic potential distribution of the motor's permanent magnet poles as shown in Fig. 2.

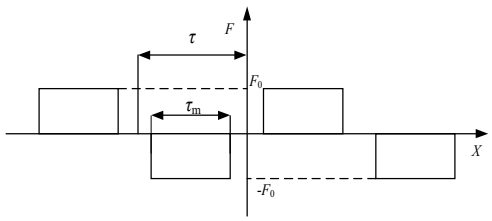

Fig. 2 Magnetic potential distribution of permanent magnetic poles

The potential distribution function F(x) of the motor can be obtained from the potential distribution. The expression is:

$$F(x)=\begin{cases} 0 & k\tau-\frac{\tau-\tau_m}{2}\le x\le k\tau+\frac{\tau-\tau_m}{2} \\ (-1)^k F_0 & k\tau+\frac{\tau-\tau_m}{2}\le x\le k\tau+\frac{\tau+\tau_m}{2} \end{cases} \tag{1}$$

$$F_0 = H_c h_m \tag{2}$$

ISSN: 2414-1895 DOI: 10.6919/ICJE.202504_11(4).0042

Hc is the coercivity, k=0, ±1, ±2,…
F(x) can be expanded from the Fourier series as:

$$F(x)=\sum_{n=1}^{\infty}\left(b_{\mathrm{n}}\sin\frac{n\pi x}{l}\right) \tag{3}$$

$$b_{\mathrm{n}}=\frac{2}{l}\int_{0}^{l}F(x)\sin\frac{n\pi x}{l}dx \tag{4}$$

Integrating Eq. (4) yields

$$b_{\mathrm{n}}=\frac{(-1)^{k}4F_{0}}{n\pi}\sin\frac{(2k+1)n\pi\tau}{2l}\sin\frac{n\pi\tau_{\mathrm{m}}}{2l} \tag{5}$$

Substituting equation (5) into equation (3) yields

$$F(x)=\sum_{n=1}^{\infty}\sin\frac{n\pi x}{l}\frac{(-1)^{k}4F_{0}}{n\pi}\sin\frac{(2k+1)n\pi\tau}{2l}\sin\frac{n\pi\tau_{\mathrm{m}}}{2l} \tag{6}$$

3.2 Specific Permeability of a Magnetic Circuit

The secondary of the motor is constructed with alternating poles and a magnetizing block is added to the primary, so the structure of the magnetic circuit changes along the x-axis. The specific permeability function can be used to express the pattern of change:

$$\Lambda(x)=\frac{\mu_{0}}{\delta(x)}=\frac{B(x)}{F(x)} \tag{7}$$

μ0 is the air permeability,δ(x) is the air gap length function, B(x) is the air gap magnetic density distribution function,F(x) is the magnetic potential function. Fig. 3 shows the specific permeability of the primary and air-gap sections.

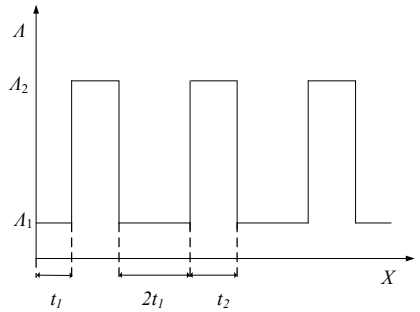

Fig. 3 Primary and air-gap specific permeability

$$\Lambda_{1}(x)=\begin{cases}\Lambda_{1} & -t_{1}+kT\le x<t_{1}+kT\\ \Lambda_{2} & t_{1}+kT\le x<t_{1}+t_{2}+kT\end{cases} \tag{8}$$

ISSN: 2414-1895 DOI: 10.6919/ICJE.202504_11(4).0042

Λ1=μ0/(h1+2g),Λ2=μ0/(2g + h1- h2), t1 and t2 are the width of the coil edges and the width of the magnetic conductive block,T=2t1+t2,k=0,1,2,…
Fig 4 shows the secondary specific permeability.

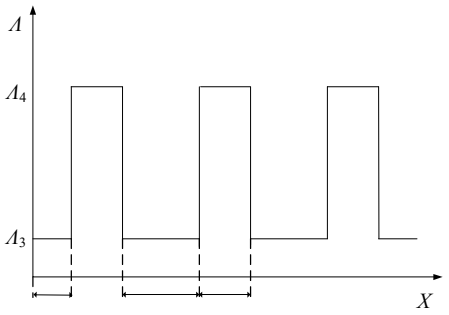

Fig. 4 Secondary specific permeability

$$\Lambda_2(x)=\begin{cases}\Lambda_3 & -t_3+kT\le x<t_4+kT\\ \Lambda_4 & t_4+kT\le x<t_3+t_4+kT\end{cases} \tag{9}$$

Λ3=μ0/(hm+hfe),Λ4=μ0/hm,t3=(τ-t4)/2,t4 is the ferromagnetic pole width, T=2t3+t4,k=0,1,2,…
Obtained from the Fourier series expansion:

$$\Lambda(x)=\sum_{n=1}^{\infty}\Lambda_n\sin\frac{n\pi x}{l} \tag{10}$$

$$\Lambda_n=\frac{2}{l}\int_0^l\Lambda(x)\sin\frac{n\pi x}{l}dx \tag{11}$$

Organize and obtain:

$$\begin{aligned}\Lambda_1(x)=&\sum_{n=1}^{\infty}\left[\frac{4\Lambda_1}{n\pi}\sin\frac{n\pi t_1}{l}\sin\frac{n\pi kT}{l}\right]\sin\frac{n\pi x}{l}\\&+\sum_{n=1}^{\infty}\left[\frac{4\Lambda_2}{n\pi}\sin\frac{n\pi t_2}{2l}\sin\frac{(2k+1)n\pi T}{2l}\right]\sin\frac{n\pi x}{l}\end{aligned} \tag{12}$$

$$\begin{aligned}\Lambda_2(x)=&\sum_{n=1}^{\infty}\left[\frac{4\Lambda_3}{n\pi}\sin\frac{n\pi t_3}{l}\sin\frac{n\pi kT}{l}\right]\sin\frac{n\pi x}{l}\\&+\sum_{n=1}^{\infty}\left[\frac{4\Lambda_4}{n\pi}\sin\frac{n\pi t_4}{2l}\sin\frac{(2k+1)n\pi T}{2l}\right]\sin\frac{n\pi x}{l}\end{aligned} \tag{13}$$

The specific permeability function is expressed as:

$$\Lambda(x)=\frac{1}{\frac{1}{\Lambda_1(x)}+\frac{1}{\Lambda_2(x)}} \tag{14}$$

ISSN: 2414-1895 DOI: 10.6919/ICJE.202504_11(4).0042

3.3 Calculation of Air Gap Magnetic Field

The unloaded air gap magnetization (radial component) can be obtained through Eq. (6) and Eq. (14).

$$B(x) = F(x)\Lambda(x) \tag{15}$$

For different relative positions between the primary and secondary of the motor, the analytical results of the analytical method are compared with those of the finite element method, as shown in Figures 5 and 6.

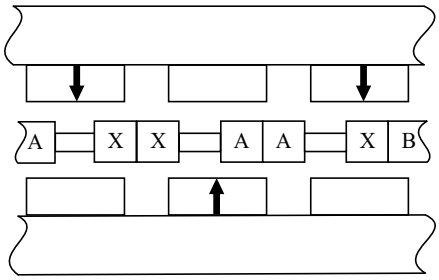

(a) Relative position of primary and secondary 1

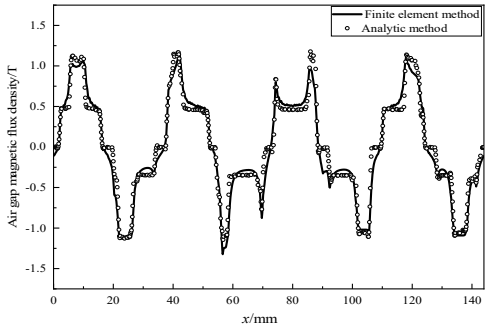

(b) No-load air gap magnetization

Fig. 5 Airborne air gap magnetic density distribution at primary and secondary relative position 1

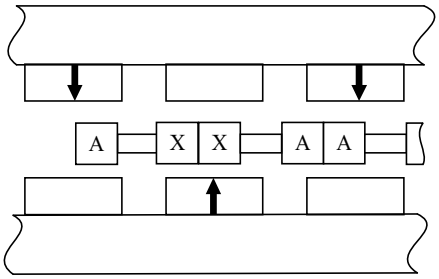

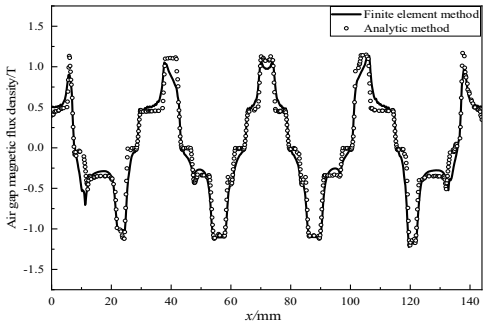

(a) Relative position of primary and secondary 2 (b) No-load air gap magnetization

Fig. 6 Airborne air gap magnetic density distribution at primary and secondary relative position 2

From Figs. 5 and 6, it can be seen that the unloaded air gap magnetization obtained by the analytical method is similar to the finite element simulation results.

3.4 Harmonic Analysis of the Air Gap Magnetization

The harmonic analysis of the no-load air gap magnetism of the motor is shown in Fig. 7.

ISSN: 2414-1895 DOI: 10.6919/ICJE.202504_11(4).0042

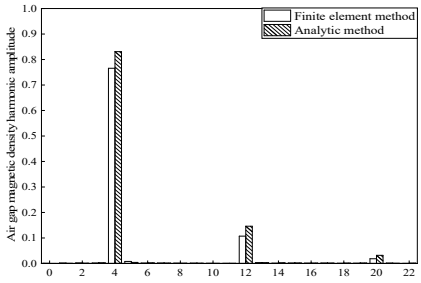

(a) No iron core

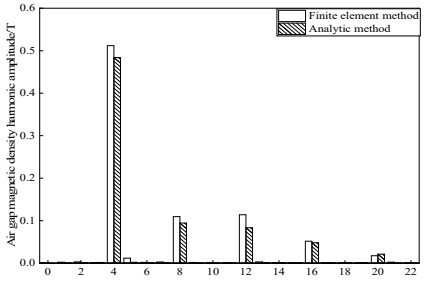

(b) Alternating poles without iron core

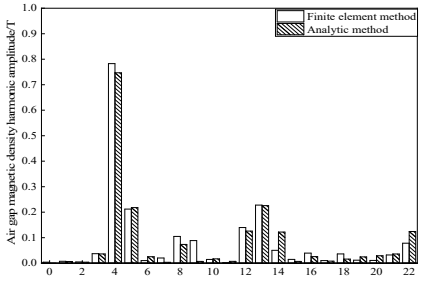

(c) Alternating poles of the primary strip-guide block

Fig. 7 Harmonic analysis of no-load air gap flux density

The motor used is an 8-pole, 9-slot structure with pole pair number p=4, whose 4th harmonic is the fundamental wave of the motor. From Fig. 7, it can be seen that the N-S-pole motor has the largest amplitude of fundamental magnetic density, which is 0.76T. In addition, the motor has high 3rd and 5th harmonic amplitudes of 0.11 T and 0.02 T, respectively. Alternating pole ironless core motors also have the largest amplitude of fundamental density with an amplitude of 0.511 T, while the 2nd, 3rd, 4th, and 5th harmonic magnetization amplitudes of the motor are relatively high. The amplitude of the fundamental-wave magnetic density of the alternating-pole ironless core motor increases to 0.78 T with the addition of a magnetic-conducting block to the primary, and the 2nd, 3rd, 4th, and 5th harmonics remain essentially unchanged, but the other higher harmonic components are elevated significantly. According to Fig. 7, it can be seen that the decrease in the amount of permanent magnets for the alternating pole motor leads to a decrease in the amplitude of the fundamental magnetization of the motor and also to a significant increase in the amplitude of the even harmonic magnetization of the motor. A comparison of motor performance is shown in Table 2.

Table 2. Comparison of motor performance

Motor	Average thrust /N	Thrust fluctuation /%
No iron core	48.87	0.16
Alternating poles without iron core	33.56	0.18
Alternating poles with magnetizing block	75.46	8.07

ISSN: 2414-1895 DOI: 10.6919/ICJE.202504_11(4).0042

As can be seen from Table 2, the thrust of the alternating-pole ironless core motor does not halve with the halving of the amount of permanent magnets, indicating that the alternating-pole structure improves the utilization of permanent magnets. The thrust of the alternating-pole motor is improved considerably with the addition of a magnetic-conducting block to the primary, but the thrust fluctuation is also increased from 0.18% to 8.07%. The incorporation of the magnetic guide block results in a large increase in the amplitude of the base wave magnetic density of the motor, thereby increasing the thrust of the motor. The addition of the magnetically conductive block simultaneously leads to an increase in the higher harmonic components of the air gap magnetic field, which makes the thrust fluctuation of the motor larger.

4. Optimized Design of the Motor

The average thrust Favg and thrust fluctuation Frip are the main measures of motor performance. In this paper, the average thrust and thrust fluctuation are used as the optimization objectives to optimize the structural parameters of the motor, and the permanent magnet pole width τm, the ferromagnetic pole width tfe, the magnetization height of the permanent magnet pole hm, the height coefficient of the magnetic conductor block kh, the width of the magnetic conductor block t2, the fillet radius of the magnetic conductor block r are selected as the optimization variables. Before motor optimization, it is necessary to understand the impact of different parameters on motor performance to lay a good foundation for the optimization work.

4.1 Influence of Structural Parameters on Motor Performance

The primary winding and current are kept constant during the following analysis.

4.1.1 Influence of the radius of the fillet of the magnetic guide block on the motor

The primary guide block is rounded as in Fig. 8.

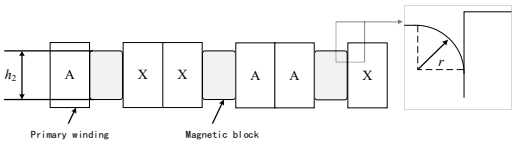

Fig. 8 Rounding of the magnetic block

Keeping the other parameters of the motor unchanged, change the fillet radius r of the magnetic guide block alone. The relationship between r and thrust and thrust fluctuation is shown in Fig. 9.

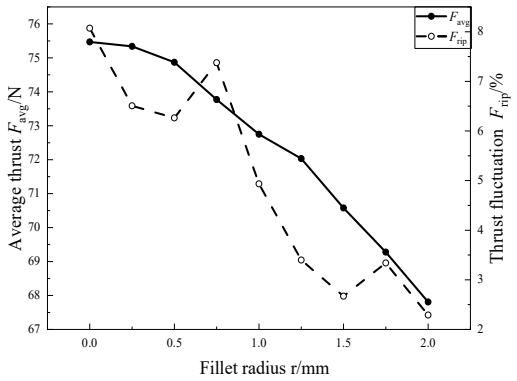

Fig. 9 Effect of the radius of the fillet of the magnetic guide block on the thrust and thrust fluctuation

ISSN: 2414-1895 DOI: 10.6919/ICJE.202504_11(4).0042

From Fig. 9, it can be seen that the thrust of the motor tends to decrease as the radius of the fillet of the magnetic guide block, r, increases. This is because an increase in the radius of the fillet reduces the amount of conductor block, which affects the magnetizing effect of the conductor block and reduces the thrust of the motor.

4.1.2 Effect of the Height Coefficient of the Magnetic Guide Block on the Motor

The height coefficient of the guide block kh represents the ratio of the height of the guide block to the height of the primary winding, h2/h1. Keeping other parameters constant, only kh is changed.The curves of thrust and thrust fluctuation versus kh are shown in Fig. 10.

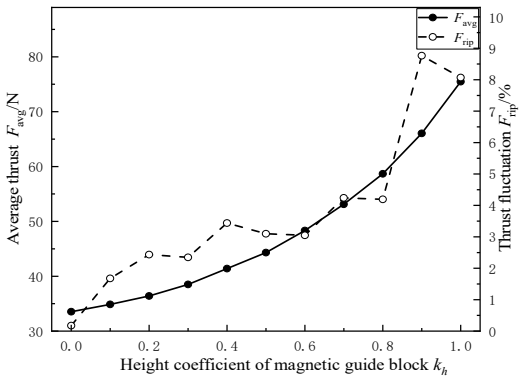

Fig. 10 Effect of the height coefficient of the magnetic guide block on thrust and thrust fluctuation

From Fig. 10, it can be seen that the output thrust of the motor increases significantly with the increase in the height factor kh of the primary magnetizing block. This is due to the fact that when the height coefficient of the magnetic guide block is increased, the amount of magnetic guide block is subsequently increased, and the gathering capacity of the primary winding is enhanced, thus boosting the thrust of the motor. Increasing the height coefficient of the magnetic guide block increases the magnetizing ability of the block, but the thrust fluctuation of the motor also increases.

4.1.3 Effect of the Width of the Magnetic Guide Block on the Motor

Keeping the electrical load constant, the cross-sectional area of the coil is unchanged, the height of the magnetic guide block h2 is equal to the height of the coil h1, and adjusting the dimensional parameter of the width of the primary magnetic guide block t2, the effect of the width of the magnetic guide block t2 on the thrust and the fluctuation of the thrust is shown in Fig. 11.

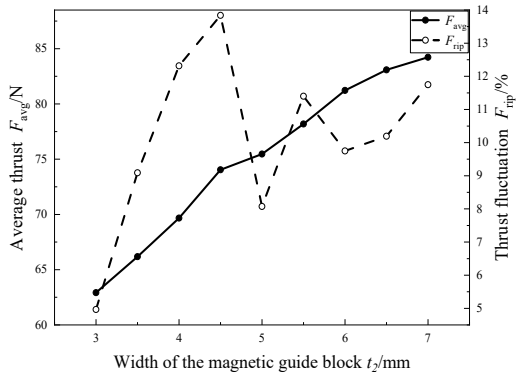

Fig. 11 Effect of the width of the magnetic guide block on thrust and thrust fluctuation

ISSN: 2414-1895 DOI: 10.6919/ICJE.202504_11(4).0042

The thrust of the motor tends to increase as the width of the magnetic guide block t2 increases. This is because when the cross-sectional area of the coil is kept constant, an increase in the width of the magnetic guide block, t2, decreases the width of the coil, t1, and the height of the coil, h1, increases, and the overall volume of the magnetic guide block becomes larger, which enhances the magnetizing ability of the block and thus increases the thrust of the motor. However, a change in the width of the permeable block t2 also causes a change in the motor flux, which in turn affects the thrust fluctuation of the motor.

4.2 Obtaining Optimization Variables based on Taguchi Method

According to the actual engineering experience and the influence of some parameters on the motor, the range of values of the optimization variables is shown in Table 3, and the height of the permanent magnet hm is always equal to the height of the convex iron pole hfe.

Table 3. Optimization variable value ranges

Variable	τ_m/mm	t_{fe}/mm	h_m/mm	k_h	t_2/mm	r/mm
Level 1	12	12	5.0	0.6	4.0	0.0
Level 2	13	13	5.5	0.7	4.5	0.25
Level 3	14	14	6.0	0.8	5.0	0.5
Level 4	15	15	6.5	0.9	5.5	0.75
Level 5	16	16	7.0	1.0	6.0	1.0

Preliminary optimization of the motor is carried out according to Taguchi's method, an orthogonal test matrix is established and the test results are obtained by finite element simulation. In order to analyze the effect of each optimization variable on the average thrust and thrust fluctuation, the finite element test results were averaged, and the average values of the optimization variables for the optimization objectives at different levels are shown in Fig. 12.

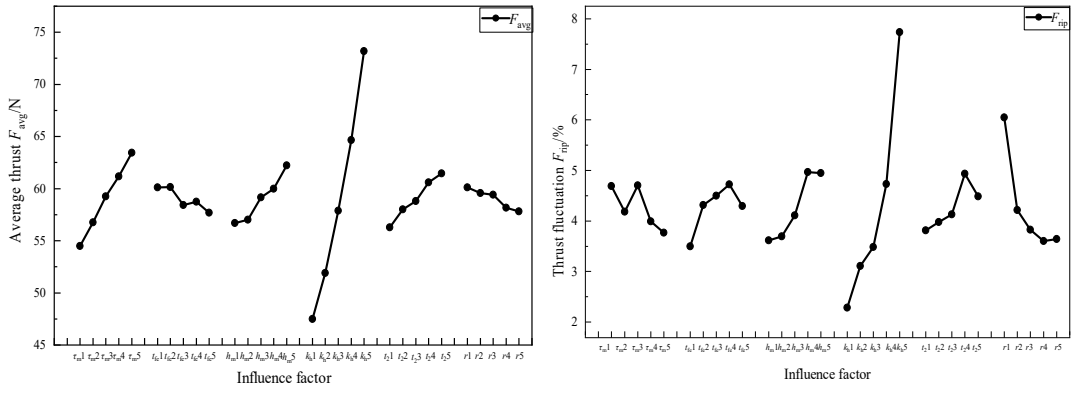

(a) Average thrust (b) Thrust fluctuation

Fig. 12 Mean values of optimization variables at different levels of the optimization objective

From Fig. 12, it can be seen that the influence of the height coefficient kh of the guide block, the width of the permanent magnet pole τm and the height of the permanent magnet hm on the thrust is large, while the height coefficient kh of the guide block, the radius of the rounding angle of the guide block r and the height of the permanent magnet pole hm have a significant effect on the fluctuation of the thrust. Under comprehensive consideration, the height coefficient of the guide block kh, the width of the permanent magnet pole τm and the radius of the rounded corner of the guide block r are selected as the main optimization variables, while other optimization variables are taken as fixed values on the basis of the results of Taguchi's experimental design, with the width of the ferrous pole

ISSN: 2414-1895 DOI: 10.6919/ICJE.202504_11(4).0042

tfe taken as 14mm, the height of the permanent magnet body hm taken as 6mm, and the width of the guide block t2 taken as 5mm.

4.3 Response Surface Methodology

Response surface method is mainly a method to find the mathematical law between the test target and each influence factor[18,19], and to find the optimal value of each factor level. The values taken for the optimization variables are classified as high level 1, central value 0, and low level -1, and the range of values for the remaining optimization variables are selected according to Taguchi's method, as shown in Table 4.

Table 4. Optimization variable level values

Optimization variables	-1	0	1
τ_m/mm	13	14	15
k_h	0.8	0.9	1
r/mm	0.25	0.5	0.75

Based on the BOX-Behnken design, the designed orthogonal test matrix is shown in Table 5.

Table 5. Orthogonal test table and test results

Number of tests	τ_m/mm	k_h	r/mm	F_{avg}/N	F_{rip}/%
1	15	0.9	0.25	68.88	4.50
2	14	1.0	0.25	75.34	6.57
3	14	1.0	0.75	73.77	6.33
4	13	1.0	0.5	71.46	7.09
5	14	0.9	0.5	65.89	4.22
6	14	0.8	0.25	59.05	3.44
7	14	0.9	0.5	65.89	4.22
8	14	0.9	0.5	65.89	4.22
9	15	0.9	0.75	67.68	2.77
10	13	0.8	0.5	56.04	3.84
11	15	0.8	0.5	61.01	3.34
12	13	0.9	0.75	62.14	3.66
13	15	1.0	0.5	77.94	7.03
14	14	0.8	0.75	58.31	2.24
15	14	0.9	0.5	65.89	4.22
16	14	0.9	0.5	65.89	4.22
17	13	0.9	0.25	63.21	4.71

The response surface method was used to find the fitting function:

$$\begin{aligned} F_{avg} = {} & 31.7579 + 5.3554\tau_m - 136.1226k_h + 10.3354r \\ & + 3.7802\tau_m \cdot k_h - 0.1335\tau_m \cdot r - 8.3077k_h \cdot r \\ & - 0.2092\tau_m^2 + 93.0478k_h^2 - 3.2737r^2 \end{aligned} \tag{16}$$

ISSN: 2414-1895 DOI: 10.6919/ICJE.202504_11(4).0042

$$\begin{aligned} F_{rip} &= 114.712 - 6.0485\tau_m - 168.4661k_h + +6.6564r \\ &+1.0959\tau_m \cdot k_h - 0.6814\tau_m \cdot r + 9.6182k_h \cdot r \\ &+0.1856\tau_m^2 + 92.2249k_h^2 - 7.8845r^2 \end{aligned} \tag{17}$$

4.4 Optimization of Motor Parameters based on Egret Swarm Optimization Algorithm

The egret flock optimization algorithm is a heuristic algorithm that combines the feeding behavior of snowy egrets and great egrets[20]. It mainly consists of three parts: sitting strategy, aggressive strategy and discriminant condition. Before applying the egret swarm optimization algorithm, it needs to be set up with variables.

The population size of the optimization algorithm is first set to 200 and the maximum number of iterations is 500. Next, the fitted functions (16) and (17) derived from the response surface method are used as objective functions, and the optimized variables and their constraints are shown in Table 4. In order to ensure that the motor thrust at the same time, its thrust fluctuations should be minimized, the resulting Pareto front plot and the selection of points as shown in Fig. 13.

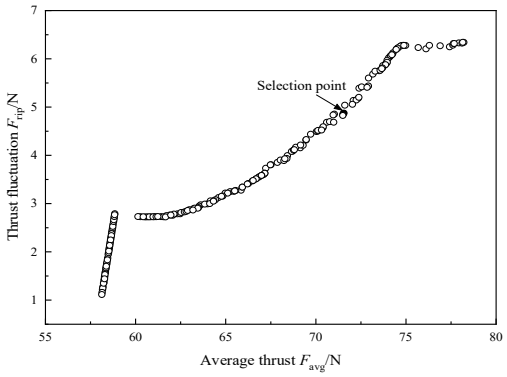

Fig. 13 Pareto Frontier Diagram

Comparison of parameters before and after optimization is shown in Table 6. After optimizing the motor parameters using the Egret swarm optimization algorithm, its average thrust is slightly reduced and the thrust fluctuation is significantly reduced.

Table 6. Comparison of parameters before and after optimization

Parameter	Before Optimization	After optimization
τ_m/mm	14	13.99
k_h	1.0	0.97
r/mm	0.0	0.59
F_{avg}/N	75.46	71.55
F_{rip}/%	8.07	4.87

The thrust waveforms of the motor in 50ms before and after optimization are obtained through finite element simulation, as shown in Fig. 14. The average thrust of the motor after optimization is 71.49N, and the thrust fluctuation is 4.96%, which is basically consistent with the results of the egret swarm optimization algorithm.

ISSN: 2414-1895 DOI: 10.6919/ICJE.202504_11(4).0042

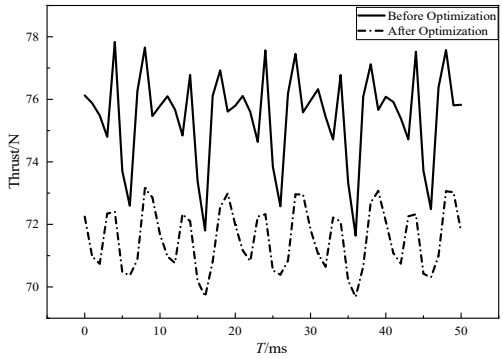

Fig. 14 Comparison of motor thrust before and after optimization

5. Conclusion

This paper proposes a permanent magnet synchronous linear motor with the addition of a magnetic guide block in the primary and an alternating pole structure in the secondary, and the following conclusions are obtained from the analysis of the motor:

(1) The no-load air-gap magnetic field of the motor is calculated by the potential distribution function of the motor as well as the specific permeability function, and the results of its analytical calculation are basically consistent with those of the finite element simulation.

(2) For the alternating-pole ironless core linear motor, the output thrust can reach 68.67% of the N-S-pole linear motor with half of the amount of permanent magnets, and its utilization of permanent magnets is higher. The addition of a magnetizing block to the primary of the motor increased its output thrust by 124.85% compared to the original, but the thrust fluctuation also increased to 8.07%.

(3) Using the egret swarm optimization algorithm for multi-objective optimization of the motor, its thrust fluctuation can be controlled at 4.87% with an average thrust reduction of 3.91N. The motor has some practical value in applications that require a certain amount of thrust and not too much precision.

References

[1] ZHU Xuhui,ZHAO Wenxiang. Research review and prospect of high-performance magnetic field modulated permanent magnet linear motor[J]. Electrical Machines and Control Applications, 2020,47(08):1-12.

[2] Jang S M, joon You D, Lee S H, et al. Design and analysis of three types for permanent magnet linear synchronous machine[C]//Sixth International Conference on Electrical Machines and Systems, 2003. ICEMS 2003. IEEE, 2003, 1: 31-33.

[3] B. Zhang, R. Qi, H. Lin. Inverse sliding mode control of laser cutting permanent magnet linear servo system[J]. Journal of Electrotechnology,2018,33(03):642-651.DOI:10.19595/j.cnki.1000-6753.tces.161675.

[4] Ma Zhenqi Research on ironless permanent magnet synchronous linear motor [D]. Southeast University, 2015.

[5] CAO R,JIN Y,ZhANG Z,et al.A new double-sided linear flux-switching permanent magnet motor with yokeless mover for electromagnetic launch system[J].IEEE Transactions on Energy Conversion,2019, 34(2):680.

[6] CHENG Yuying, LI Jiangui, YU Tianqi, et al. Study on thrust fluctuation of permanent magnet linear synchronous motor based on compensated winding[J]. Combined Machine Tools and Automatic Machining Technology,2024,(05):96-99.DOI:10.13462/j.cnki.mmtamt.2024.05.020.

[7] Boduroglu A, Demir Y, Cumhur B, et al. A novel track structure of double-sided linear PM synchronous motor for low cost and high force density applications[J]. IEEE Transactions on Magnetics, 2020, 57(2): 1-5.

ISSN: 2414-1895 DOI: 10.6919/ICJE.202504_11(4).0042

[8] Zhu Z Q, Pang Y, Howe D, et al. Analysis of electromagnetic performance of flux-switching permanent-magnet machines by nonlinear adaptive lumped parameter magnetic circuit model[J]. IEEE Transactions on magnetics, 2005, 41(11): 4277-4287.

[9] L. Li, D. Pan and X. Huang, "Analysis and Optimization of Ironless Permanent-Magnet Linear Motor for Improving Thrust," in *IEEE Transactions on Plasma Science*, vol. 41, no. 5, pp. 1188-1192, May 2013, doi: 10.1109/TPS.2013.2245425.

[10] LIU Hengkun,ZHANG Xiao,MI Zhu. Traction and normal force analysis of hollow and Halbach permanent magnet linear synchronous motors[J]. Journal of National University of Defense Technology, 2012,34(03):94-9.

[11] Wang Li. Research on key control technology of modern linear motor and its application [D]. Zhejiang University,2012.

[12] Tapia J A, Leonardi F, Lipo T A. Consequent-pole permanent-magnet machine with extended field-weakening capability[J]. IEEE Transactions on Industry Applications, 2003, 39(6): 1704-1709.

[13] Zhou Y, Shi C, Qu R, et al. A novel consequent-pole modular-mover linear permanent magnet vernier machine for thrust ripple and cost reduction[J]. IEEE Transactions on Industry Applications, 2021, 57(6): 5841-5850.

[14] S. -U. Chung *et al*., "A Feasibility Study on a New Doubly Salient Permanent Magnet Linear Synchronous Machine," in *IEEE Transactions on Magnetics*, vol. 46, no. 6, pp. 1572-1575, June 2010, doi: 10.1109/TMAG.2010.2042284.

[15] XU Xiaozhuo,SUN Zhen,WANG Xudong,et al.Characterization of Halbach alternating-pole permanent magnet synchronous linear motor[J]. Journal of Electrotechnology,2019,34(09):1825-1833.DOI:10.19595/j.cnki.1000-6753.tces.L8056.

[16] MU Zhongcui, SU Yi, ZHANG Lei, et al. Characterization and optimal design of trapezoidal Halbach alternating pole coreless permanent magnet synchronous linear motor[J]. Journal of Electrical Machines and Control,2024,28(01):164-176.DOI:10.15938/j.emc.2024.01.01.

[17] Pang Gucai, Deng Zhiquan, Zhang Zhongming. Analytical calculation of no-load air-gap magnetic field of surface-mounted permanent magnet motor based on improved generalized magnetic circuit method[J]. Journal of Electrotechnology,2019,34(22):4623-4633.

[18] Xuanfeng Shangguan,Siyuan Jiang,Jingle Zhou. Design algorithm and multi-objective optimization of double squirrel cage permanent magnet induction motor[J]. Journal of Coal,2017,42(S2):611-618.

[19] HUANG H L, ZHANG J, ZHANG C. Multi-objective optimization design of U-PMVLM based on response surface method[C]// 2023 IEEE 18th Conference on Industrial Electronics and Applications (ICIEA), China: IEEE,2023:992-997.

[20] Chen Z Y, ADAM F, Li S, et al. Egret Swarm Optimization Algorithm: An Evolutionary Computation Approach for Model Free Optimization [J]. Biomimetics,2022,7(4):144.